IEEE Access
Multidisciplinary ⋮ Rapid Review ⋮ Open Access Journal

Received 7 December 2022, accepted 22 December 2022, date of publication 2 January 2023, date of current version 5 January 2023.

Digital Object Identifier 10.1109/ACCESS.2022.3233629

RESEARCH ARTICLE

Research on Pilot Protection for Tie Line of Renewable Energy Sources

QINGHUA LAI[1], ZHE ZHANG[1], KANJUN ZHANG[2], XIANGGEN YIN[1], (Senior Member, IEEE), AND YONGXIN CHEN[2]

[1]State Key Laboratory of Advanced Electromagnetic Engineering and Technology, Huazhong University of Science and Technology, Wuhan 430074, China
[2]Hubei Electric Power Research Institute, Wuhan 430074, China

Corresponding author: Qinghua Lai (laiqhhust@163.com)

ABSTRACT With the continuous increase in the proportion, renewable energy sources have brought great challenges to the traditional protection based on fundamental frequency, due to their complex short-circuit current characteristics which are different from synchronous generators. As the main protection of the tie line (outgoing line) of the renewable energy station, the differential protection will also be seriously affected in terms of its operation performance, and even the operation failure or maloperation may occur in some cases. This paper proposes a new principle of pilot protection based on cosine similarity comparison by analyzing the fault characteristics of renewable energy sources. With the full current as the main criterion and the current fault component as the auxiliary criterion, this principle comprehensively utilizes the time domain information of the current on both sides of the line to improve the protection sensitivity. At the same time, a method of capacitive current compensation for the sampling value is proposed according to the algorithm characteristics of similarity comparison, to prevent the protection maloperation in the case of external faults. The simulation results show that, compared with the existing pilot protection based on similarity comparison, the new protection principle proposed in this paper has good engineering application value by identifying internal and external faults in a more reliable and sensitive manner.

INDEX TERMS Pilot protection, similarity, tie line, renewable energy source, wind farm.

NOMENCLATURE

Abbreviations	
RES	Renewable energy source.
LVRT	Low voltage ride through.
DC	Direct current.
PLL	Phase locked loop.
PWM	Pulse width modulation.
Symbols	
ω	Synchronous angular velocity.
ω_r	Angular frequency corresponding to rotor speed.
s	Slip.
T_{sp}	Sampling period.
T_w	Time window.
T	Fundamental frequency cycle.
Subscripts	
d, q	d/q -Axis of rotation.
S, W	System/RES side.
Φ (a, b, c)	Three phases (ABC).
f	Fault point.
Δ	Fault component.

The associate editor coordinating the review of this manuscript and approving it for publication was Gab-Su Seo.

I. INTRODUCTION

In order to reduce the fossil energy consumption and environmental impact, the renewable energy power generation technologies represented by photovoltaic power generation and wind power generation have been continuously developing for a long time [1], [2]. In addition, with the proposal of carbon neutrality goals in various countries, the grid-connected power generation capacity of renewable energy will further increase [3], [4], [5], [6], [7]. For large-scale renewable energy power plants, the RES is generally connected to the power grid through tie lines (outgoing lines)

after being collected by collector lines. As an important channel connecting the RES with the power grid, the safe and stable operation of the tie line is very important.

Due to the structural characteristics and LVRT control strategy, the RES provides the short-circuit current with different characteristics from the synchronous generator, such as limited amplitude, large phase change range, and frequency offset [8], [9]. Such complex fault characteristics make it difficult for the traditional pilot distance protection and pilot direction protection to be applied to renewable energy tie lines. The existing tie lines basically use the current differential protection as the main protection. When the short-circuit current provided by the RES is much smaller than the short-circuit current provided by the system, a good adaptability can be ensured for the current differential protection. However, with the gradual increase in the proportion of RESs, the influence of the fault characteristics of RESs on the current differential protection has become increasingly prominent: in the case of an internal fault of the tie line, the phase angle difference between the currents on both sides may be greater than 90 degrees. When the magnitudes of the short-circuit currents on both sides are close to each other, the sensitivity of the differential protection will be significantly reduced, and even the operation failure will occur [10], [11], [12].

In response to the above problems, some scholars have studied the new principle of pilot protection suitable for renewable energy occasions. Reference [13] used the difference between current amplitudes on both sides of the line to construct the pilot protection scheme, but the protection performance is greatly affected by the proportion of connected RESs. References [14] and [15] proposed the principle of pilot protection based on positive sequence fault components, which still relies on the calculation of power frequency phasors. However, the transient adjustment process of short circuit current of RES and other frequency components that may be included in the fault current, such as the rotor speed frequency component provided by the doubly fed induction generator after the crowbar is triggered, may lead to errors in the extraction of power frequency components and affect the performance of this method. Reference [16] constructed the pilot protection scheme by confirming whether the differential voltage and differential current across the line conform to the capacitance model, so the calculation accuracy will be affected by the non-power frequency. What's more, the voltage information on the opposite side is required, which reduces the pilot protection reliability to a certain extent. References [17], [18], [19], [20], and [21] proposed a variety of pilot protection principles based on waveform similarity comparison according to the difference between short-circuit currents on both sides of the tie line. However, there are many deficiencies in the current intensity selection, time window selection, protection setting, etc. in the absence of in-depth analysis on the protection operation characteristics, which affect the sensitivity and reliability of the protection operation. In addition, the above methods ignored the influence of capacitive current, which may cause the external maloperation.

To solve these problems, this paper firstly analyzes the short-circuit current characteristics of various RESs and their influence on traditional differential protection, and proposes a pilot protection principle based on cosine similarity comparison on this basis. Compared with the current similarity comparison criterions which are composed of full short-circuit current, the auxiliary criterion is constituted by introducing the fault component of short-circuit current. What is more, by combining with the reasonable selection of time window, the protection sensitivity can be effectively improved. In addition, a capacitive current compensation for the current sampling values on both sides of the line is proposed, which can effectively prevent the protection maloperation in the case of external faults. The simulation and experiment results verify the good performance of the proposed pilot protection principle.

This paper is organized as follows. The fault characteristics of different types of RESs and their influence on differential protection are analyzed in section II. Then in section III, a new method of pilot protection based on cosine similarity comparison is proposed. The influences of fundamental and non-fundamental components of short-circuit current, and different lengths of time window on cosine similarity are analyzed in this section, too. Solutions are proposed for practical application problems such as capacitive current compensation and unilateral power supply in section IV. On the basis of the above research, a comprehensive scheme of pilot protection based on cosine similarity is proposed. The scheme is verified by simulation and experiment in section V and VI, respectively. Finally, section VII presents the conclusion.

II. ANALYSIS OF RENEWABLE ENERGY FAULT CHARACTERISTICS AND THEIR INFLUENCE ON DIFFERENTIAL PROTECTION

According to the grid connection method and the impact on external power grid, the RESs can be divided into two basic types: inverter power source and doubly-fed power source. The former mainly includes the photovoltaic power supply, direct-driven wind turbine, etc., while the latter mainly includes the doubly-fed induction generator.

A. ANALYSIS OF FAULT CHARACTERISTICS OF INVERTER POWER SOURCE

The inverter power source is directly connected to the grid through the inverter [22], [23], with the short-circuit current characteristics mainly depending on the LVRT control strategy. In the case of a power grid fault, the inverter power source generally disconnects the voltage outer loop, and the short-circuit current is mainly controlled by the current inner loop. The block diagram of the control system after the outer loop is disconnected is shown in Fig. 1.

According to the grid code standard for fault voltage ride through [24], the inverter power source needs to provide

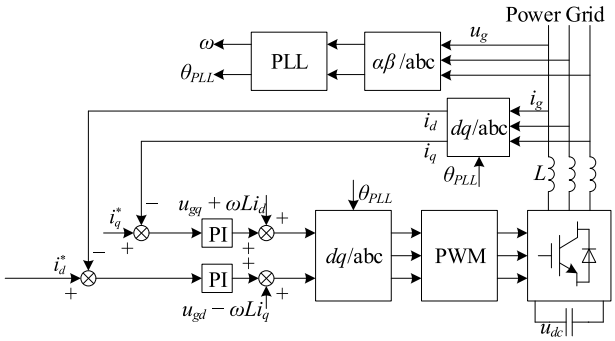

FIGURE 1. Control system after the outer loop is disconnected.

reactive current to the power grid during the fault, and tries to provide active current without overcurrent. It is assumed that the current amplitude limit is $I_{\max}$, the per-unit reference currents i_d^* and i_q^* of d and q axes of the current inner loop:

$$\begin{cases} i_d^* & = \min(P/V_1, \sqrt{I_{\max}^2 - (i_q^*)^2}) \\ i_q^* & = 1.5(0.9 - V_1) \end{cases} \tag{1}$$

where P represents the active power, and V_1 represents the positive sequence voltage. On the premise that the d-axis is oriented to the positive sequence voltage vector [25], the d-axis and q-axis currents actually reflect the magnitude of the active and reactive power.

Before the fault occurs, the RES generally only provides active power, with the q-axis current of 0. In the case of a second-order control system, the short-circuit current during a three-phase fault is [26]:

$$\begin{cases} i_d & = i_d^* - (i_d^* - P)\dfrac{e^{-\xi\omega_n t}\sin(\omega_n\sqrt{1-\xi^2}t+\beta)}{\sqrt{1-\xi^2}} \\ i_q & = i_q^* - i_q^*\dfrac{e^{-\xi\omega_n t}\sin(\omega_n\sqrt{1-\xi^2}t+\beta)}{\sqrt{1-\xi^2}} \end{cases} \tag{2}$$

where ξ represents the damping ratio of the control system, and ω_n is the natural oscillation angular frequency, both of which are related to the control parameters and inverter parameters of the PI current inner loop; and β is the damping angle, $\arctan^2\beta = (1-\xi^2)/\xi^2$.

Since the decay time constant of the decaying component in (2) is very small, the transient component can decay to zero quickly. Therefore, the transient process of short-circuit current can be ignored [27], [28], that is, the inverter power source can be approximated to enter the steady state directly, with the d-axis and q-axis currents:

$$\begin{cases} i_d & \approx i_d^* \\ i_q & \approx i_q^* \end{cases} \tag{3}$$

In the case of an asymmetric short circuit fault, the reference values of d-axis and q-axis reference currents are still given by (1). At this time, the transient process of short-circuit current can still be ignored, and (3) is still satisfied. Therefore, under various fault conditions, the inverter power source basically only provides positive sequence the short-circuit current [29], [30], and the short-circuit current equation under the three-phase (ABC) coordinate system is as follows:

$$i_\phi = i_d^*\cos(\omega t + \alpha_{i\phi}) - i_q^*\sin(\omega t + \alpha_{i\phi}) \tag{4}$$

where $\alpha_{i\Phi}$ represents the initial phase angle after the fault.

It can be seen that the basic characteristics of the short-circuit current fed by the inverter power source are that the amplitude is limited and only positive sequence current is provided. In addition, the fundamental phase of the current (phase difference with respect to the positive sequence voltage of the inverter port) ranges from 0° ($i_q = 0$) to 90° ($i_d = 0$).

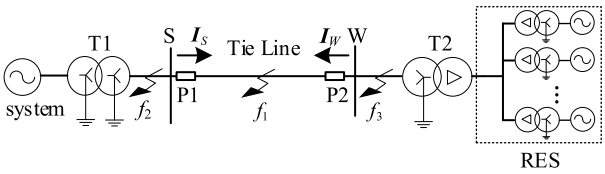

FIGURE 2. Schematic diagram of tie line of renewable energy source.

The RESs are generally connected to the power grid through tie lines, as shown in Fig. 2. In Fig. 2, the dashed box RES represents the renewable energy power plant, including multiple power generation units; T1 and T2 represent the transformers; $\boldsymbol{I}_{\mathrm{W}}$ and $\boldsymbol{I}_{\mathrm{S}}$ represent the current on the RES side and system side respectively; P1 and P2 represent the protections.

The fault characteristics of the system side are mainly determined by the traditional synchronous generator, and an equivalent form (series connection of constant voltage source and resistor) can be considered for the short-circuit calculation, with the short-circuit current equation provided as below [31]:

$$i_\phi = C_1\cos(\omega t + \theta_{i\phi}) + C_2 e^{-t/T_a} \tag{5}$$

where C_1 and C_2 are the amplitudes of the fundamental frequency component and decaying DC component, respectively, and T_a is the decay time constant.

According to the above analysis, due to the large phase change range of the short-circuit current fed by the inverter power source, the phase difference between the fundamental frequency components of the short-circuit currents on both sides of the line may increase significantly in the case of an internal fault of the tie line. The situation will be more serious when an asymmetric short circuit occurs inside the tie line: for example, in the case of a two-phase short circuit fault, the inverter power source only provides the positive sequence current without negative sequence component, the distribution characteristics of the short-circuit currents on both sides of the line will change accordingly, and the phase difference between the short-circuit currents will further increase, which will seriously affect the performance of the differential protection.

The internal two-phase fault of the tie line shown in Fig. 2 is taken as an example to analyze the phase angle relationship

between the short-circuit currents on both sides. When a two-phase (BC) fault occurs on the tie line (at f_1), and if only the fundamental frequency is considered, the fault current phasor diagram can be obtained from (3) and (5), as shown in Fig. 3.

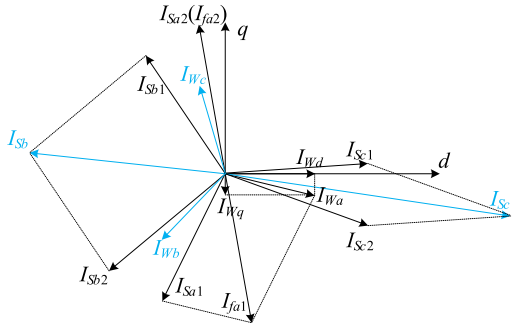

FIGURE 3. Current phasor diagram of inverter power source tie line in the case of a bc fault.

In Fig. 3, the subscripts 1 and 2 represent the positive and negative sequence components respectively. According to (3) and (4), the inverter power source only provides the positive sequence short-circuit current, so the negative sequence current at the fault point will be all provided by the system side, that is, $\boldsymbol{I}_{Sa2}$ is equal to $\boldsymbol{I}_{fa2}$. In addition, the negative sequence impedance angle is basically equal to the positive sequence impedance angle on the system side (generally 80°-90°), so the angle between $\boldsymbol{I}_{Sa2}$ and d-axis will exceed 90°. In the case of a two-phase (BC) fault, for the fault point, the boundary conditions are $\boldsymbol{I}_{fa} = 0$, $\boldsymbol{I}_{fb} = \boldsymbol{I}_{fc}$, and $\boldsymbol{U}_b = \boldsymbol{U}_c$, so it can be obtained that:

$$I_{fa1} = I_{fa2} \tag{6}$$

Since the phase with the current $\boldsymbol{I}_{Wa}$ lagging behind the d-axis on the RES side is between 0° and 90°, the A-phase positive sequence current $\boldsymbol{I}_{Sa1}$ on the system side can be obtained according to the parallelogram law ($\boldsymbol{I}_{Sa1} = \boldsymbol{I}_{fa2} - \boldsymbol{I}_{Wa}$), and thus the short-circuit current of A/B/C phase on both sides.

The analysis of Fig. 3 shows that with the change of the magnitude and angle of $\boldsymbol{I}_{Wa}$, the phase angle difference between the B-phase currents on both sides will never exceed 90°, but the angle between the C-phase (the lagging-phase) currents $\boldsymbol{I}_{Wc}$ and $\boldsymbol{I}_{Sc}$ will change greatly: when $\boldsymbol{I}_{Wa}$ is close to the q-axis current component $\boldsymbol{I}_{Wq}$, the angle difference between the C-phase currents on both sides is close to zero; however, the smaller the angle between $\boldsymbol{I}_{Wa}$ and d-axis, the closer the amplitudes of I_{Wa} and I_{Sa1}, and the larger the angle difference between the C-phase currents on both sides, which may even exceed 90°. According to relevant studies on the stability of the power grid with RESs, the inverter power source connected to the grid will not be able to operate stably [32], [33], [34], [35], [36], when the short circuit ratio of the system is less than 2. It can be approximately assumed that the amplitude ratio of I_{Wa} to I_{Sa1} is 1:2, that the positive sequence impedance angle on the system side is 80°-90°, and that the angle between I_{Wa} and d-axis is zero, so the range of the maximum angle between $\boldsymbol{I}_{Wc}$ and $\boldsymbol{I}_{Sc}$ can be obtained:

$$\varphi_{c\max} \in (125°, 134°) \tag{7}$$

This shows that in the case of a two-phase short-circuit fault, the maximum phase angle difference between the lagging phase currents may reach 134°, which is much larger than that when both sides of the line are powered by synchronous generators.

B. ANALYSIS OF FAULT CHARACTERISTICS OF DOUBLY-FED POWER SOURCE

1) ANALYSIS OF SHORT-CIRCUIT CURRENT CHARACTERISTICS UNDER THE ACTION OF EXCITATION REGULATION

The doubly-fed power source is generally equipped with a crowbar protection [37], with its fault current characteristics directly related to the operation of the crowbar protection. In the case of crowbar protection failure, the short-circuit current characteristics of the doubly-fed power source are mainly affected by the LVRT control strategy [38], [39]. In current practical engineering applications, the doubly-fed induction generator system is similar to the inverter power source, which mainly adopts the LVRT control strategy of negative sequence current suppression, that is, only the positive sequence current is provided. At this time, the short-circuit current provided by the doubly-fed power source can be expressed as:

$$i_\phi = A_1 \cos(\omega t + \beta_{i\phi}) + A_2 e^{-t/T_d} \tag{8}$$

where A_1 and A_2 are the amplitudes of the fundamental frequency component (positive sequence) and decaying DC component, respectively, and T_d is the decay time constant.

The comparison between (8) and (4) reveals that the phase angle relationship between the fundamental frequency components of the short-circuit currents on both sides can still be analyzed by Fig. 3, with the conclusion similar to that of the inverter power source: in the case of an internal asymmetric short circuit of the tie line, the phase difference between the fundamental frequency components of the short circuit currents on both sides may exceed 90°.

2) ANALYSIS OF SHORT-CIRCUIT CURRENT CHARACTERISTICS AFTER CROWBAR PROTECTION OPERATION

Since the tie line is directly connected to the main transformer of the renewable energy power plant, the crowbar protection will be easily activated in the case of a tie line fault, especially an interphase short circuit. At this time, the short-circuit current provided by the doubly-fed power source can be expressed as [40]:

$$i_\phi = B_1 \cos(\omega t + \gamma_{i\phi}) + B_2 e^{\frac{-t}{T_s}} + B_3 e^{\frac{-t}{T_r}} \cos(\omega_r t + \gamma_{ir\phi}) \tag{9}$$

where T_s and T_r are the decay time constants of DC component and speed frequency component, respectively;

B_1-B_3 are the amplitudes. Equation (9) shows that after the crowbar protection operation, the short-circuit current provided by the doubly-fed power source includes the fundamental frequency component, decaying speed frequency component and decaying DC component. Obviously, the speed frequency component will significantly affect the accuracy of power frequency extraction.

When only the fundamental frequency component is considered, the two-phase (BC) fault at f_1 in Fig. 2 is taken as an example (analogy analysis is acceptable for other fault types) to analyze the phase angle difference between the currents on both sides.

When only the fundamental frequency component is calculated, the doubly-fed power source is actually an asynchronous motor, with its equivalent impedances in the positive-sequence and negative-sequence networks shown as below:

$$\begin{cases} Z_{(1)} & = j\omega L_{s\sigma} + (j\omega L_{r\sigma} + R_r/s) \,||\, j\omega L_m \\ Z_{(2)} & = j\omega L_{s\sigma} + (j\omega L_{r\sigma} + R_r/(2-s)) \,||\, j\omega L_m \end{cases} \tag{10}$$

where $L_{s\sigma}$ and $L_{r\sigma}$ are the leakage inductances of the stator and rotor; L_m is the mutual inductance between stator and rotor; R_r is the equivalent resistance of the rotor; and s is the slip, taken as $(-0.3, 0.3)$. Obviously, the impedance angle for equivalent impedance in (10) is related to s and $Z_{(2)} < Z_{(1)}$, where $Z_{(2)}$ is less affected by s and close to the typical impedance angle on the system side, while $Z_{(1)}$ is significantly affected by s. When $s < 0$ before the fault, the phasor diagram of the fault current is shown in Fig. 4.

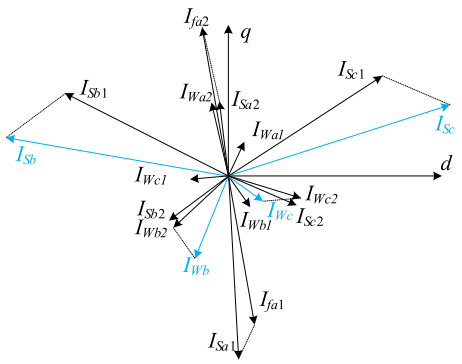

FIGURE 4. Current phasor diagram of doubly-fed power source tie line in the case of a bc fault (When crowbar protection is triggered).

In Fig. 4, the short circuit current I_W provided by the RES also contains the negative sequence component, and the phases of $\boldsymbol{I}_{Wa2}$ and $\boldsymbol{I}_{Sa2}$ are close to each other. Since the mutual inductance L_m in (10) is much larger than the leakage inductance L_σ, $\boldsymbol{I}_{Wa1}$ is always close to the q-axis when s changes. When $I_{Wa1} < I_{Wa2}$ (due to $Z_{(2)} < Z_{(1)}$) and the angle between $\boldsymbol{I}_{Wa1}$ and d-axis is between (45°, 90°), the angle between $\boldsymbol{I}_{Wb}$ and $\boldsymbol{I}_{Sb}$ and the angle between $\boldsymbol{I}_{Wc}$ and $\boldsymbol{I}_{Sc}$ are less than 90° according to the phasor diagram.

Similarly, if slip $s > 0$, $\boldsymbol{I}_{Wa1}$ will be on the left of the q-axis and close to the q-axis, but the above conclusion still holds.

To sum up, in the case of a tie line fault, the phase difference between the fundamental frequency components of the short-circuit currents on both sides of the line is generally less than 90° after the operation of the crowbar protection. However, it should be noted that the speed frequency component contained in the short-circuit current will seriously affect the phase calculation accuracy of the fundamental frequency component, which will increase the phase difference, thus degrading the protection performance based on the fundamental frequency component.

3) APPLICABILITY ANALYSIS OF DIFFERENTIAL PROTECTION

Based on the Kirchhoff's current law, the principle of current differential protection has a good performance and is one of the main protections commonly used in transmission lines. At present, the differential protection based on the fundamental frequency component is generally adopted as the main protection of the tie line in renewable energy plant. Taking the system shown in Fig. 2 as an example, the typical operation equation of the current differential protection is:

$$|I_W + I_S| \geq K_{res} \, |I_W - I_S| \tag{11}$$

where $\boldsymbol{I}_W$ and $\boldsymbol{I}_S$ represent the current phasors on the RES and system sides respectively (calculated by the full-cycle Fourier algorithm); K_{res} is the braking coefficient. The forward direction of current is from the busbar to the line, as shown in Fig. 2.

According to the geometric knowledge, the equality between both sides of (11) indicates the differential protection critical state, which is represented as a circle on the complex plane, see circle C_1 in Fig. 5 for details.

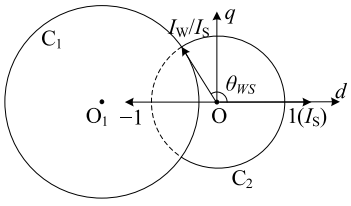

FIGURE 5. Schematic diagram of differential protection operation zone.

In Fig. 5, $\boldsymbol{I}_S$ is positioned on the real axis, and the phasors are subject to the per-unit transformation based on I_S. Circle C_1 (center is O_1) is the coordinate trajectory of $\boldsymbol{I}_W$ on the complex plane when both sides of criterion (11) are exactly equal, and the outside of the circle is the operation zone of this criterion. Assuming that the current amplitude on the system side is larger than that on the RES side (i.e., $I_S > I_W$), circle C_2 is the trajectory of I_W on the complex plane under different phase differences.

For the low proportion of connected RESs, the short-circuit current I_W on the RES side is small, C_2 and C_1 overlap to a small extent or even does not overlap with each other, and the differential protection almost never fails. As the proportion of RESs increases (the ratio of I_W to I_S increases), the radius of C_2 will increase, and gradually overlap C_1 (dotted line).

If the phase difference θ_{WS} exceeds a certain value, the phasor $\boldsymbol{I}_W/\boldsymbol{I}_S$ will enter C_1, causing the differential protection to fail.

Therefore, the high proportion of RESs will significantly reduce the sensitivity of the traditional current differential protection, and even cause the operation failure. It is necessary to study and propose a new pilot protection principle to better ensure the safety of power grid operation.

In order to improve the sensitivity of tie line pilot protection, a feasible way is to provide the pilot protection by comparing the waveform difference (similarity) between short-circuit currents on both sides of the line. When an external short-circuit fault occurs, the same current flows on both sides of the line, with exactly the same short-circuit current waveform (excluding the influence of capacitive current and measurement error); when an internal fault occurs, there is a significant difference between the short-circuit current waveforms on both sides (the difference is the current at the fault point), so that the internal and external faults can be distinguished. Compared with the traditional current differential protection based on the fundamental frequency component, the pilot protection principle based on the waveform similarity comparison can make full use of the full short-circuit current information such as fundamental and non-fundamental frequency components, so as to effectively improve the protection sensitivity. On the other hand, there is no need to extract the fundamental frequency component, the protection is less affected by the LVRT control transient characteristics of the RES and the speed frequency component generated under the crowbar protection of the doubly-fed induction generator system, which helps to further improve the protection performance.

III. NEW PRINCIPLE OF PILOT PROTECTION BASED ON COSINE SIMILARITY COMPARISON

A. SELECTION OF SIMILARITY ALGORITHM

There are many algorithms for measuring waveform similarity [41], and the typical methods commonly used mainly include Pearson correlation coefficient method, Euclidean distance method and cosine similarity comparison method. Assuming that the forward direction of the current is from the busbar to the line (as shown in Fig. 2), and the sampling values of the current waveforms on both sides of the tie line are $\boldsymbol{x} = [x_1, x_2, \ldots, x_n]$ and $\boldsymbol{y} = [y_1, y_2, \ldots, y_n]$, then the similarity equations between $\boldsymbol{x}$ and $\boldsymbol{y}$ calculated by Pearson correlation coefficient, Euclidean distance and cosine similarity are:

$$p(x,y) = \frac{\sum_{i=1}^{n}(x_i-\bar{x})(y_i-\bar{y})}{\sqrt{\sum_{i=1}^{n}(x_i-\bar{x})^2}\sqrt{\sum_{i=1}^{n}(y_i-\bar{y})^2}} \tag{12}$$

$$euc(x,y) = \sqrt{\sum_{i=1}^{n}(x_i+y_i)^2} \tag{13}$$

$$\cos(x,y) = \frac{\sum_{i=1}^{n}x_i y_i}{\sqrt{\sum_{i=1}^{n}x_i^2}\sqrt{\sum_{i=1}^{n}y_i^2}} \tag{14}$$

where $\bar{x}$ and $\bar{y}$ represent the arithmetic mean of the data in $\boldsymbol{x}$ and $\boldsymbol{y}$, respectively; $x_i + y_i$ in (13) corresponds to assumption that the forward direction of current is from the busbar to the line. Obviously, $euc(\boldsymbol{x}, \boldsymbol{y}) \geq 0$, and both $p(\boldsymbol{x}, \boldsymbol{y})$ and $\cos(\boldsymbol{x}, \boldsymbol{y})$ range between -1 and 1. When $\boldsymbol{x}$ is completely opposite to $\boldsymbol{y}$, $x_i + y_i \approx 0$, and the theoretical calculation values for the above similarity algorithms reach the minimum.

For the Pearson correlation coefficient $p(\boldsymbol{x}, \boldsymbol{y})$, the sampling value is centralized (that is, the sampling value is arithmetically averaged), so the convergence rate will be slightly slower in theory, and the range of $p(\boldsymbol{x}, \boldsymbol{y})$ is difficult to directly analyze by the current characteristic equation in the case of an internal fault, thus making the protection setting difficult. In addition, $p(\boldsymbol{x}, \boldsymbol{y})$ is more suitable for linear correlation applications.

If the sampling values $\boldsymbol{x}$ and $\boldsymbol{y}$ are regarded as the multi-dimensional space vectors, the Euclidean distance $euc(\boldsymbol{x}, \boldsymbol{y})$ is to describe the difference by the distance between the space vectors. Due to the great effect by the $\boldsymbol{x}$ and $\boldsymbol{y}$ dimensions, the range of calculated value is unstable compared with $\cos(\boldsymbol{x}, \boldsymbol{y})$. In addition, for sine function applications, $euc(\boldsymbol{x}, \boldsymbol{y})$ is of relatively higher sensitivity when the difference between the current amplitudes on both sides is large, while in the case of small currents, the method based on phase characteristic comparison is more sensitive in principle.

The cosine similarity $\cos(\boldsymbol{x}, \boldsymbol{y})$ is an algorithm that evaluates the similarity according to the cosine value of the angle between multi-dimensional space vectors. For short-circuit currents $x(t)$ and $y(t)$ that change with time, if the calculation time is z, (14) can be rewritten as follows:

$$f(z) = \frac{\sum_{i=1}^{n}x(z+iT_{sp})y(z+iT_{sp})}{\sqrt{\sum_{i=1}^{n}x^2(z+iT_{sp})}\sqrt{\sum_{i=1}^{n}y^2(z+iT_{sp})}} \tag{15}$$

where n is the number of sampling points contained in the time window T_w, and $n = T_w/T_{sp}$. When T_{sp} is small enough, (15) can be converted into cosine similarity in integral form:

$$f(z) = \frac{\int_z^{z+T_w}x(t)y(t)dt}{\sqrt{\int_z^{z+T_w}x^2(t)dt}\sqrt{\int_z^{z+T_w}y^2(t)dt}} \tag{16}$$

Assuming that $x(t)$ and $y(t)$ are the one-dimensional sine waves, i.e. $A\sin(\omega t)$ and $B\sin(\omega t + \varphi)$ respectively, and assuming that the time window (integration time) T_w is the cycle T of sine wave, by substituting them into (16), it can be obtained that:

$$\frac{\int_0^T A\sin(\omega t)B\sin(\omega t+\varphi)dt}{\sqrt{\int_0^T A^2\sin^2(\omega t)dt}\sqrt{\int_0^T B^2\sin^2(\omega t+\varphi)dt}} = (AB\pi\cos\varphi)/(AB\pi) = \cos\varphi \tag{17}$$

It is not difficult to prove that (17) is still true when the time window is T/2. So $\cos(\boldsymbol{x}, \boldsymbol{y})$ is essentially the cosine of the angle between the space vectors $\boldsymbol{x}$ and $\boldsymbol{y}$. Since the short-circuit current generally can be expressed as the superposition of sinusoidal quantities of different frequencies (or damped sinusoidal quantities), $\cos(\boldsymbol{x}, \boldsymbol{y})$ operation characteristics in different fault conditions can be easily analyzed and evaluated according to the short-circuit current characteristics, so as

to facilitate the rational setting of protection setpoint, and the improvement of protection performance through effective measures according to the analysis result. Therefore, this paper chooses cosine similarity comparison as the basic algorithm to construct the pilot protection.

B. ANALYSIS OF INFLUENCE OF FAULT CHARACTERISTICS ON COSINE SIMILARITY METHOD

The cosine similarity actually reflects the phase relationship after the synthesis of different components. The following sections analyze the influence of the fundamental frequency component and non-fundamental frequency component on the cosine similarity comparison algorithm respectively.

1) INFLUENCE OF FUNDAMENTAL FREQUENCY COMPONENT

a: INVERTER POWER SOURCE

According to (17), when the currents on both sides are sine functions of the same frequency, the cosine similarity reflects the phase angle difference between the currents. As can be seen from the analysis in Fig. 3, when a two-phase short circuit occurs on the tie line, the maximum phase angle difference between the C-phase (lagging phase) currents may reach 134°. In order to improve the protection sensitivity, an effective measure is to compare the cosine similarity based on the variation of short circuit current (fault component).

Note that when the angle between $\boldsymbol{I}_{Wa}$ and d-axis is small, the situation where the angle between $\boldsymbol{I}_{Wc}$ and $\boldsymbol{I}_{Sc}$ is larger than 90° is the most serious. Assuming that the load current provided by the RES before the fault is I_P, and the difference between the current and I_P after the fault is the short-circuit current component, the C-phase current fault component phasor diagram shown in Fig. 6 can be obtained from Fig. 3.

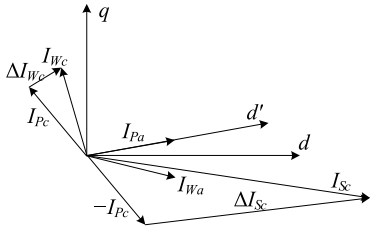

FIGURE 6. Fault component phasor diagram of c-phase current in the case of inverter power source.

In Fig. 6, the d' axis represents the positive sequence voltage vector position obtained by the PLL before the fault occurs, and the d-axis lags behind the d' axis [14]; ΔI_{Wc} and ΔI_{Sc} represent the fault components of the C-phase currents on both sides. When the angle between $\boldsymbol{I}_{Wa}$ and d-axis is small, the amplitudes of I_{Wa} and I_{Pa} are close to each other, and the phase angle of the variation ΔI_{Wa} of the A-phase current on the RES side is about $-90°$, so the angle between ΔI_{Wc} and ΔI_{Sc} will be significantly smaller than 90°.

Based on the above analysis, it can be seen that in the case of a two-phase (BC) fault, when I_{Wa} is close to q-axis, the phase angle difference between the C-phase currents on both sides is less than 90°; when I_{Wa} gradually approaches d-axis, the phase angle difference between the fundamental frequency components of the C-phase currents on both sides will be close to or even greater than 90°, but the phase angle difference between the fault components of the C-phase currents on both sides will be significantly less than 90°. For the B-phase current, the phase angle difference is less than 90° regardless of full current or fault component.

For other types of short-circuit faults, the above-mentioned similar analysis method shows that the phase angle difference between the short-circuit current variations of the faulty phases on both sides is less than 90°. Therefore, using the fault component of short-circuit current for cosine similarity comparison will help to improve the protection sensitivity.

b: DOUBLY-FED POWER SOURCE UNDER THE ACTION OF EXCITATION REGULATION

When the crowbar protection is not operated, the short-circuit current provided by the doubly-fed power source is shown in (8).It can be seen from the comparison between (8) and (4) that when only the fundamental frequency component is considered, the influence of fault current on the calculated cosine similarity can still be analyzed by the phasor diagram shown in Fig. 3 and Fig. 6, and the analysis conclusion is similar to that for the inverter power source.

c: DOUBLY-FED POWER SOURCE AFTER CROWBAR PROTECTION IS TRIGGERED

In Fig. 4, the phase angle difference between the fundamental frequency components of the short-circuit currents under the two-phase (BC) fault has been analyzed, and it can be concluded that the phase angle difference between the currents on both sides is always less than 90°. The analysis similar to that in Fig. 6 shows that the angle between the fault components of the currents on both sides is also less than 90°. The above conclusions also apply to other types of short-circuit faults.

To sum up, the sensitivity of protection can be effectively improved to prevent the protection from failing, by using the fault component of short-circuit current for cosine similarity comparison.

Like the traditional protection, the cosine similarity comparison method based on the fault component can only be applied to practical engineering for a short time. Therefore, the full currents and fault components on both sides can be used to construct the pilot protection, with the cosine similarity comparison based on the full current as the main criterion and the cosine similarity comparison based on the fault component as the auxiliary criterion, to improve the protection sensitivity when the phase angle difference between the currents on both sides is greater than 90°.

2) INFLUENCE OF NON-FUNDAMENTAL FREQUENCY COMPONENT

The pilot protection based on the cosine similarity comparison will use the full short-circuit current information

(including fundamental and non-fundamental frequency components) for the fault judgment, so as to improve the protection sensitivity. The following sections analyze the influence of the non-fundamental frequency component on the cosine similarity comparison for different RESs.

a: INVERTER POWER SOURCE

For the tie line connected to the inverter power source, only the short-circuit current provided by one side (system side) contains the decaying DC component according to (4) and (5). When the time window T_w is T (T is the fundamental frequency cycle), by substituting $A\sin(\omega t)$ and $B\sin(\omega t+\varphi)+C$ into (16), $f(z)$ is:

$$f(z) == \frac{B\pi\cos\varphi}{\sqrt{\pi}\sqrt{B^2\pi + C^2T}} = \cos\varphi/\sqrt{1+\frac{C^2T}{B^2\pi}} \quad (18)$$

In the actual short-circuit current, due to the short cycle T, the calculation result of $f(z)$ in (18) is about $\cos\varphi$, that is, the constant DC component C has no significant influence on the calculation result of $f(z)$. In other words, if T_w is set to T, there is no significant improvement on the protection performance by the difference between the DC components in the short-circuit current values on both sides of the line. When C is the decaying DC component, $f(z)$ presents a certain fluctuation as shown in curve 1 (dashed line) in Fig. 7.

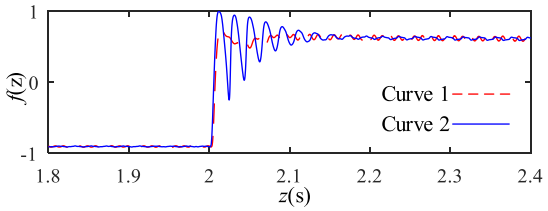

FIGURE 7. Influence of one-side decaying dc component on calculated cosine similarity.

If T_w is set to T/2, $f(z)$ is:

$$f(z) = \frac{\int_z^{z+T/2} x(t)y(t)dt}{\sqrt{\int_z^{z+T/2} x^2(t)dt}\sqrt{\int_z^{z+T/2} y^2(t)dt}} \quad (19)$$

By substituting $x(t) = A\sin(\omega t)$ and $y(t) = B\sin(\omega t+\varphi)+C$ into (19), $f(z)$ is:

$$f(z) = \frac{\cos\varphi + \frac{4C}{B\pi\omega}\cos(\omega z)}{\sqrt{1+\frac{8C}{B\pi\omega}\cos(\omega z+\varphi)+\frac{C^2T}{B^2\pi}}} \quad (20)$$

and $f(z+\mathrm{T}) = f(z)$. Compared with (18), it can be seen that when T_w is set to T/2, the calculation result of $f(z)$ is related to z and shows a sinusoidal periodic variation with constant amplitude.

Assuming that $z_1 = (\pi/2-\varphi)/\omega$ and $z_2 = (3\pi/2-\varphi)/\omega$, by substituting them into (20), the following can be obtained:

$$f(z_1) = (\cos\varphi + \frac{4C}{B\pi\omega}\cos(\frac{\pi}{2}-\varphi))/\sqrt{1+\frac{C^2T}{B^2\pi}} \quad (21)$$

$$f(z_2) = (\cos\varphi + \frac{4C}{B\pi\omega}\cos(\frac{3\pi}{2}-\varphi))/\sqrt{1+\frac{C^2T}{B^2\pi}} \quad (22)$$

Obviously, no matter what the symbolic relationship between B and C is, there must be one in $f(z_1)$ and $f(z_2)$ that is greater than the calculation result given by (18) when the time window is T. In the actual short-circuit current, the DC component C will gradually decay to zero (i.e., decaying DC component). At this time, the sinusoidal fluctuation of the calculation result of $f(z)$ will become smaller and smaller, which will eventually be equal to (17), namely, $\cos\varphi$. The variation process is shown in curve 2 (solid line) in Fig. 7.

The Fig. 7 shows that the maximum of curve 2 (solid line) is larger than that of curve 1. In other words, compared with the time window is set to T, setting the time window T_w to T/2 will effectively increase the calculation value of cosine similarity, which is beneficial to make use of the difference between the DC components of the short-circuit currents on both sides and improve the protection sensitivity.

For the external fault (or non-faulty phase), when the capacitive current is ignored, $x(t)$ is basically opposite to $y(t)$. By substituting $y(t) = -x(t)$ into (19), it can be obtained:

$$f(z) = \frac{-\int_z^{z+T/2} x^2(t)dt}{\sqrt{\int_z^{z+T/2} x^2(t)dt}\sqrt{\int_z^{z+T/2} x^2(t)dt}} = -1 \quad (23)$$

This shows that $f(z)$ is basically unaffected by different frequency components, and the calculated result is always -1. This conclusion holds for different time windows.

It can be seen from the above analysis that when the short-circuit current value contains the decaying DC component, the cosine similarity algorithm should adopt the 1/2 fundamental frequency time window (the corresponding time window is 10 ms when the rated grid frequency is 50 Hz) to make better use of the difference between the DC components on both sides to improve the protection sensitivity. On the one hand, the forward fluctuation generated by the T/2 time window can be used to increase the calculated cosine similarity during an internal fault, thereby improving the protection sensitivity. On the other hand, compared with the conventional algorithm adopting the fundamental frequency cycle time window, the T/2 time window can also effectively improve the protection operation speed and promote the fault elimination.

b: DOUBLY-FED POWER SOURCE UNDER THE ACTION OF EXCITATION REGULATION

According to (5) and (8), the short circuit currents on both sides of the tie line contain the decaying DC component. For the external fault, if the influence of capacitor current is ignored, the currents on both sides are of the same magnitude and opposite direction, with the calculated cosine similarity of -1, which is similar to the case of inverter power source. For the internal fault, it is assumed that both $x(t)$ and $y(t)$ contain only fundamental frequency current and constant DC component, which are $A\sin(\omega t)+D$ and $B\sin(\omega t+\varphi)+C$,

respectively. When the integration time in (16) is T, the following can be obtained by substituting $x(t)$ and $y(t)$ into it:

$$f(z) = \frac{\int_z^{z+T}(A\sin(\omega t)+D)(B\sin(\omega t+\varphi)+C)dt}{\sqrt{\int_z^{z+T}(A\sin(\omega t)+D)^2dt}\sqrt{\int_z^{z+T}(B\sin(\omega t+\varphi)+C)^2dt}} = \frac{AB\pi\cos\varphi+CDT}{\sqrt{A^2\pi+D^2T}\sqrt{B^2\pi+C^2T}} \quad (24)$$

In (24), the denominator is always positive, while for the numerator, CDT is always greater than zero because the initial values C and D of the aperiodic components of the short-circuit currents on both sides of the line have the same sign (same polarity) when the internal short circuit occurs, which indicates that the existence of aperiodic components will shift the calculated cosine similarity to the positive direction (especially when $AB\pi\cos\varphi$ is less than zero), and make it away from the calculated value in the case of a reverse fault (the calculated value is negative in the case of a reverse fault), thus improving its sensitivity in response to an internal fault.

It should be noted that when T in $f(z)$ is changed to T/2, the calculation result of $f(z)$ will fluctuate periodically, as shown below:

$$f(z) = \frac{AB\pi\cos\varphi+4BD\frac{\cos(\omega z+\varphi)}{\omega}+}{\sqrt{A^2\pi+8AD\frac{\cos(\omega z)}{\omega}+D^2T}\cdot} \times \frac{4AC\frac{\cos(\omega z)}{\omega}+CDT}{\sqrt{B^2\pi+8BC\frac{\cos(\omega z+\varphi)}{\omega}+C^2T}} \quad (25)$$

Like the analysis in Equations (20) and (18), the forward amplitude of $f(z)$ is increased (compared with (24)) when the time window is changed from T to T/2 in (25), which is conducive to improving the protection sensitivity and operation speed. When the decay of aperiodic components is taken into account, the above periodic fluctuation will gradually decrease, but the T/2 time window can still improve the protection sensitivity.

c: DOUBLY-FED POWER SOURCE AFTER CROWBAR PROTECTION IS TRIGGERED

According to (9), the short-circuit current provided by the doubly-fed power source after the crowbar protection contains the decaying DC component and decaying rotating-speed frequency component.

For the decaying DC component, the signs of C_2 and B_2 in (5) and (9) are the same when the internal fault occurs on the tie line, that is, the same polarity of the current decaying DC components on both sides. According to (24) and (25), the decaying DC component is conductive to improving the protection sensitivity at this time.

The decaying rotating-speed frequency component only exists in the fault current provided by the RES side. Assuming that $x(t)$ is $A\sin(\omega t)$ and $y(t)$ is $B\sin(\omega t+\varphi)+B'\sin(\omega_r t+\varphi')$, after substitution into (19), the decaying rotating-speed frequency component on one side will cause the repeated oscillation of the calculated cosine similarity and the oscillation amplitude will decrease gradually with the decay of the rotating-speed frequency component, which is similar to the case when only one side contains the decaying DC component. The above oscillation occurs when the time window is of fundamental frequency cycle T and T/2. Like the one-side decaying DC component in the inverter power source condition, if the time window is set to T/2, the forward amplitude of $f(z)$ can be effectively increased, with the protection sensitivity and operation rotating-speed further improved.

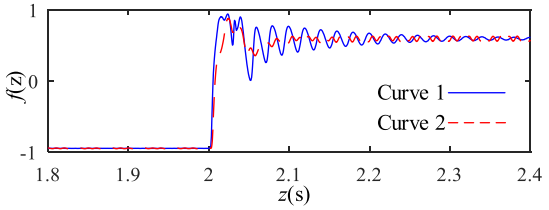

FIGURE 8. Influence of decaying rotating-speed frequency component on cosine similarity under different time windows.

Fig. 8 shows the influence of single-side decaying rotating-speed frequency component on the cosine similarity calculation result of faulty phase under different time windows. The time window corresponding to curve 1 (solid line) is T/2, and that corresponding to curve 2 (dotted line) is T. The comparison between oscillations of curve 1 and curve 2 in Fig. 8 reveals that the oscillation amplitude is higher when the time window is T/2, which is more conducive to improving the protection sensitivity.

IV. PILOT PROTECTION SCHEME BASED ON COSINE SIMILARITY

According to the analysis of the influence of RES fault characteristics on the cosine similarity algorithm, the pilot protection based on the cosine similarity comparison can adopt a comprehensive protection scheme combining full short-circuit current and fault component, supplemented by a reasonable selection of time window (T/2 time window), which can effectively improve the protection sensitivity. On the other hand, due to the limited current amplitude of the RES in practical engineering applications, the proportion of capacitive current is relatively high in the case of an external fault of the tie line, especially the external fault on the system side, so measures need to be taken to prevent the protection maloperation. In addition, when the tie line is powered by a single power source (e.g., in the case of a decommissioned renewable energy power plant), an internal fault of the tie line will cause the cosine similarity comparison method to fail since there may be no short-circuit current on one side of the line, so effective countermeasures also need to be taken to ensure the reliable protection operation and fault elimination.

This section will firstly provide the capacitive current compensation method of the pilot protection and the protection

strategy in the case of a single power source, and propose the specific construction scheme of pilot protection on this basis.

A. CAPACITIVE CURRENT COMPENSATION SCHEME

In the traditional current differential protection based on the fundamental frequency component, the phasor-based capacitive current compensation method is mainly used. However, for the pilot protection principle based on the cosine similarity comparison, the current sampling value (instantaneous value) is used for calculation, so it is unsuitable for the phasor-based capacitive current compensation method and a new capacitive current compensation method is required.

For the direct compensation on the current sampling value, the method of symmetrical components is no longer applicable, and the modulus calculation can be used for the three-phase decoupling. The Clarke transformation is used in this paper to decompose the three-phase system into $\alpha\beta$ *0* moduli to achieve the purpose of decoupling [42], [43].

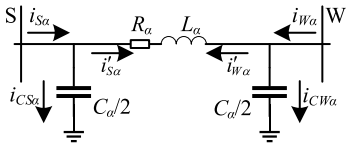

FIGURE 9. II-shaped equivalent circuit at α-modulus.

The equivalent circuit of each modulus of the tie line adopts the II-shaped equivalent circuit. Among which, the tie line II-shaped equivalent circuit at α-modulus is shown in Fig. 9, with C_α, R_α and L_α representing the capacitance, resistance and inductance of the α-modulus equivalent circuit respectively. Equivalent circuits at β and *0* moduli are similar. According to the II-shaped equivalent circuit, each modulus current compensated by capacitor current can be calculated (for example, the α-modulus currents $i'_{S\alpha}$ and $i'_{W\alpha}$ in Fig. 9), and then the ABC three-phase currents compensated by capacitor current can be calculated by Clarke inverse transformation. Taking the RES side (W side) as an example to illustrate the capacitive current compensation method, which is similar to the compensation method of the system side.

Firstly, the sampling values $i_{W-abc}(k)$ and $u_{W-abc}(k)$ of the three-phase current and voltage at a certain time k are transformed into $\alpha\beta 0$ moduli through the Clarke transformation:

$$\begin{cases} \boldsymbol{i}_{W-\alpha\beta 0}(k) & = \boldsymbol{C}\boldsymbol{i}_{W-abc}(k) \\ \boldsymbol{u}_{W-\alpha\beta 0}(k) & = \boldsymbol{C}\boldsymbol{u}_{W-abc}(k) \end{cases} \tag{26}$$

where $\boldsymbol{i}_{W-abc}(k)$ and $\boldsymbol{u}_{W-abc}(k)$ represent the column matrices formed by the three-phase current and voltage sampling values; $\boldsymbol{i}_{W-\alpha\beta 0}(k)$ and $\boldsymbol{u}_{W-\alpha\beta 0}(k)$ represent the current and voltage column matrices at $\alpha\beta 0$ moduli; $\boldsymbol{C}$ is the Clarke transformation matrix:

$$\boldsymbol{C} = \frac{1}{3}\begin{bmatrix} 2 & -1 & -1 \\ 0 & 3^{1/2} & -3^{1/2} \\ 1 & 1 & 1 \end{bmatrix} \tag{27}$$

Then, the capacitive current is compensated according to the II-shaped equivalent circuit at $\alpha\beta 0$ moduli. For example, after the capacitive current compensation, the W-side current $i_{W\alpha}(k)$ at α-modulus is:

$$i'_{W\alpha}(k) = i_{W\alpha}(k) - \frac{C_\alpha}{2}\frac{d(u_{W\alpha}(k) - u_{W\alpha}(k-1))}{dt} \tag{28}$$

Similarly, the compensated currents at β and *0* moduli can be obtained and formed into the current matrix $i'_{W-\alpha\beta 0}(k)$.

The three-phase current sampling value after compensation can be obtained through the Clarke inverse transformation of $i'_{W-\alpha\beta 0}(k)$:

$$\boldsymbol{i'}_{W-abc} = \boldsymbol{C}^{-1}\boldsymbol{i'}_{W-\alpha\beta 0} \tag{29}$$

where $\boldsymbol{C}^{-1}$ is the inverse matrix corresponding to (29). Then the cosine similarity can be calculated by using the compensated current sampling value.

B. HANDLING OF POWER SUPPLY BY UNILATERAL POWER SOURCE

When only one side of the tie line is supplied with power, if a short fault occurs in the tie line, the passive side will not provide short-circuit current. For example, if the renewable energy source is out of operation for some reason, the fault current i_W is about zero. In this case, the cosine similarity algorithm cannot calculate normally, and the calculation result may be wrong. This may lead to the failure of the cosine similarity comparison method, resulting in protection fail. To handle the situation, a feasible solution is to determine whether there is a short circuit fault in the tie line by taking advantage of the fact that there is a large short circuit current on one side of the line and the short circuit current on the other side is basically zero. The specific method is as follows.

Assuming that $i'_{S\phi}$ and $i'_{W\phi}$ are the phase current sampling values on both sides after the capacitor current compensation, that whether the sampling current reach the threshold value is judged by:

$$\begin{cases} \sum_{i=1}^{n} |i'_{S\phi-i}| & > I_{setz} \\ \sum_{i=1}^{n} |i'_{W\phi-i}| & > I_{setz} \end{cases} \tag{30}$$

where I_{setz} is the zero-current threshold setpoint and can be set as $0.08I_n$ (I_n is the rated current). The time window is T/2.

When (30) is satisfied, the similarity comparison criterion is used; if (30) does not hold, the following criteria can be used to determine whether there is an internal fault:

$$\begin{cases} \max(\sum_{i=1}^{n} \left|i'_{S\phi-i}\right|, \sum_{i=1}^{n} \left|i'_{W\phi-i}\right|) > I_{setz} \\ (\sum_{i=1}^{n} \left|i'_{S\phi-i}\right| > 2\sum_{i=1}^{n} \left|i'_{W\phi-i}\right|) \\ \cup(\sum_{i=1}^{n} \left|i'_{W\phi-i}\right| > 2\sum_{i=1}^{n} \left|i'_{S\phi-i}\right|) \end{cases} \tag{31}$$

Once (31) is satisfied, the protection will be triggered.

C. MAIN CRITERIA AND IMPLEMENTATION PROCESS OF PILOT PROTECTION

In order to improve the protection sensitivity, the full currents and fault components on both sides are used to construct the pilot protection based on cosine similarity, the criteria are:

$$r_{\phi} = \frac{\sum_{i=1}^{n} i'_{S\phi-i} i'_{W\phi-i}}{\sqrt{\sum_{i=1}^{n} (i'_{S\phi-i})^2} \sqrt{\sum_{i=1}^{n} (i'_{W\phi-i})^2}} > c_{set} \quad (32)$$

$$r_{\Delta\phi} = \frac{\sum_{i=1}^{n} i'_{S\Delta\phi-i} i'_{W\Delta\phi-i}}{\sqrt{\sum_{i=1}^{n} (i'_{S\Delta\phi-i})^2} \sqrt{\sum_{i=1}^{n} (i'_{W\Delta\phi-i})^2}} > c_{set-\Delta} \quad (33)$$

where c_{set} and $c_{set-\Delta}$ represent the setpoints of the criteria based on full current and fault component, respectively; r_{Φ} and $r_{\Delta\Phi}$ represent the corresponding calculation results respectively; and the time window is taken as T/2.

According to the above analysis, the ideal calculation values of (32) and (33) are both -1 when an external short-circuit fault occurs on the tie line. Therefore, the setpoints c_{set} and $c_{set-\Delta}$ shall be between -1 and 0. In order to give consideration to the sensitivity and safety of the protection, c_{set} and $c_{set-\Delta}$ can be set as -0.5. This leaves a high margin for the reliability of protection in the case of both internal and external faults.

To sum up, the implementation steps of the pilot protection scheme proposed in this paper are shown in Fig. 10.

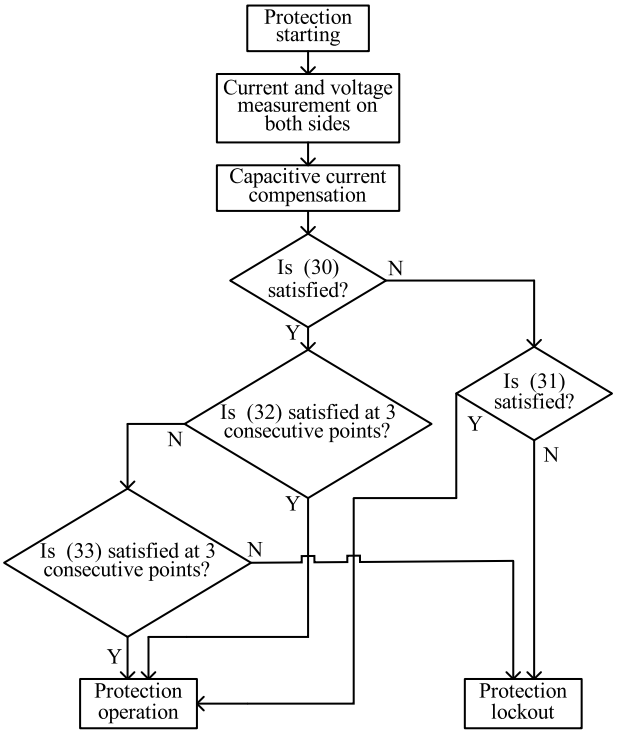

FIGURE 10. Flow chart of pilot protection scheme.

V. SIMULATION VERIFICATION AND ANALYSIS

In order to verify the effectiveness of the pilot protection scheme proposed in this paper, PSCAD/EMTDC is used to build the simulation model of the power grid shown in Fig. 2 for the simulation verification in the case of different fault locations (f_1-f_3), different fault types and different RESs.

TABLE 1. Parameters of tie line.

Sequences	Resistances	Inductive Reactance	Capacitive Reactance
Positive Sequence	0.04 Ω/km	0.281 Ω/km	269 MΩ*m
Zero Sequence	0.138 Ω/km	0.688 Ω/km	396 MΩ*m

Relevant parameters of the simulation model are as follows: The renewable energy power plant contains multiple power generation units with a total capacity of 90 MVA and a rated frequency of 50 Hz. The type of RES can be adjusted as needed; the voltage class of the system-side transformer T1 is 500/220 kV; the main transformer T2 is 100 MVA in rated capacity, 220/35 kV in rated voltage, and 6.22% in short-circuit impedance; the tie line is 150 km long, and uses the distributed parameter model, with the parameters shown in Table 1. Unless otherwise specified, the time window and sampling frequency for the protection is 10 ms and 1 kHz respectively.

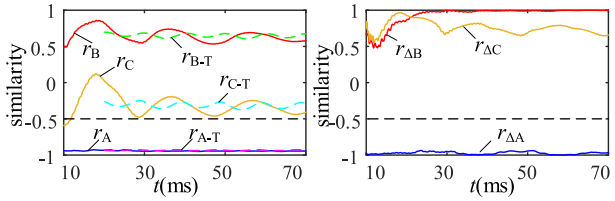

FIGURE 11. Simulation results in the case of an internal bc fault on tie line of inverter power source.

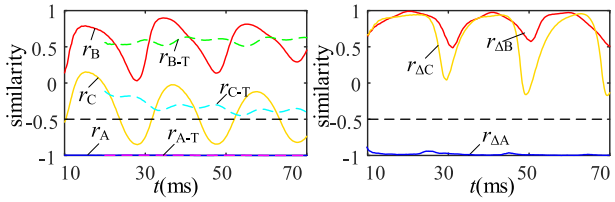

FIGURE 12. Simulation results in the case of an internal bc fault on tie line of doubly-fed power source.

A. SIMULATION RESULTS FOR DIFFERENT RENEWABLE ENERGY SOURCES

Fig. 11 and Fig. 12 are the examples of simulation results of the protection calculation values in the case of an internal two-phase (BC) fault of the tie line (that is, at f_1 in Fig. 2) for the inverter power source and the doubly-fed power source (without crowbar protection operation): the fault occurs at 0 ms, data are valid after 10 ms; the rated power is provided by the RES before the fault occurs; the dotted straight line shows the setpoint of the protection criterion; r represents

TABLE 2. Protection operation simulation results for inverter power source.

Fault type	Maximum value in 10-20 ms interval after fault						Result at 20 ms after fault			Operation phase	Operation time
	r_A	r_B	r_C	$r_{\Delta A}$	$r_{\Delta B}$	$r_{\Delta C}$	$r_{A\text{-}T}$	$r_{B\text{-}T}$	$r_{C\text{-}T}$		
f_{1AG}	0.988	−0.999	−0.999	0.999	−0.998	−0.999	0.914	−0.998	−0.998	A	12 ms
f_{1BC}	−0.956	0.923	0.223	−0.964	0.868	0.967	−0.967	0.831	−0.261	BC	12 ms
f_{1BCG}	−0.999	0.974	0.769	−0.999	0.941	0.883	−0.999	0.523	0.733	BC	12 ms
f_{1ABC}	0.998	0.999	0.975	0.759	0.878	0.948	0.998	0.931	0.734	ABC	12 ms
f_{2AG}	−0.945	−0.968	−0.969	−0.883	−0.905	−0.924	−0.995	−0.995	−0.927	none	/
f_{2BC}	−0.993	−0.992	−0.995	−0.991	−0.849	−0.975	−0.996	−0.999	−0.998	none	/
f_{2BCG}	−0.865	−0.958	−0.992	−0.914	−0.978	−0.985	−0.981	−0.998	−0.998	none	/
f_{2ABC}	−0.874	−0.884	−0.921	−0.860	−0.842	−0.903	−0.997	−0.958	−0.941	none	/
f_{3AG}	−0.997	−0.995	−0.997	−0.996	−0.996	−0.997	−0.998	−0.995	−0.999	none	/
f_{3BC}	−0.942	−0.949	−0.987	−0.964	−0.957	−0.984	−0.998	−0.998	−0.990	none	/
f_{3BCG}	−0.983	−0.989	−0.998	−0.985	−0.991	−0.998	−0.997	−0.999	−0.998	none	/
f_{3ABC}	−0.974	−0.997	−0.997	−0.976	−0.998	−0.997	−0.995	−0.999	−0.998	none	/

the cosine similarity calculation result; the subscripts A, B and C represent the three phases, and Δ represents the fault component. In addition, Fig. 11 and Fig. 12 also give the calculated cosine similarity of the full current when the protection adopts a 20 ms time window, which is marked with the subscript -T.

In Fig. 11, r_A and $r_{\Delta A}$ are significantly less than the setpoint of −0.5 after 10 ms, and the A-phase (non-fault phase) protection will not act. For the B-phase protection, r_B and $r_{\Delta B}$ are always significantly higher than the setpoint after 10 ms, and the protection can operate reliably. For the C-phase (lagging phase) protection, the r_C at 10 ms is close to the setpoint of −0.5 (since the phase angle difference between the fundamental frequency currents on both sides is greater than 90°, which is consistent with the theoretical analysis result) that is lack of sensitivity. However, $r_{\Delta C}$ is much larger than the setpoint and the protection can still operate reliably. Assuming that the condition for protection operation is that the calculation results at 3 consecutive points meet the criteria, under the sampling frequency of 1 kHz, the acting time of B- and C-phase protections is 12 ms.

For doubly-fed power source, as shown in Fig. 12, the A-phase protection does not operate under an internal BC fault, while the B-phase protection operates reliably. For the C-phase protection, which is similar to that for the inverter power source shown in Fig. 11, the cosine similarity of the fault component ($r_{\Delta C}$) has a higher sensitivity, and the protection can still operate reliably.

In addition, from the comparison of r_A and r_{A-T}, and r_B and r_{B-T} in Fig. 11 and Fig. 12, it can be seen that the T/2 time window can improve the protection sensitivity, which is consistent with the theoretical analysis result.

Fig. 13 and Fig. 14 show the simulation results of protection calculation values in the case of internal and external three-phase faults of the tie line for the doubly-fed power source (crowbar protection is triggered). According to Fig. 13, r_A, r_B and r_C all meet the criterion (32) at three

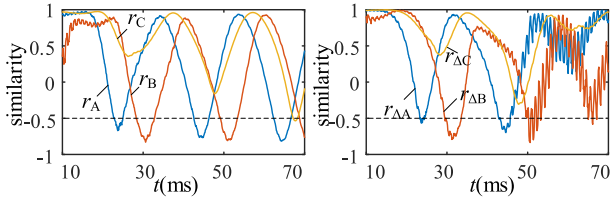

FIGURE 13. Simulation results in the case of an internal three-phase fault at f_1 of doubly-fed power source.

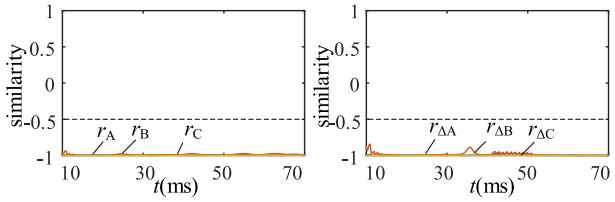

FIGURE 14. Simulation results in the case of an external three-phase fault at f_2 of doubly-fed power source.

consecutive points after 10 ms, and A-phase, B-phase and C-phase protections operate at 12 ms. According to Fig. 13, the protection does not operate in a reliable way in the case of an external fault.

The protection operation results in the case of different metallic short-circuit faults at f_1-f_3 are shown in Table 2 and Table 3, in which Table 2 is for the inverter power source, and Table 3 is for the doubly-fed power source (with crowbar protection operation). In Table 2 and Table 3, r represents the calculated cosine similarity; the subscripts A, B and C represent the three phases, Δ represents the fault component, -T represents the 20 ms time window; and the protection operation time refers to the time when the criteria are met at three consecutive points. It can be seen that the proposed pilot protection scheme can operate correctly under different short-circuit faults. In addition, the comparison between the maximum value of the faulty phase r_Φ in the 10-20 ms

TABLE 3. Protection operation simulation results for doubly-fed power source.

Fault type	Maximum value in 10-20 ms interval after fault						Result at 20 ms after fault			Operation phase	Operation time
	r_A	r_B	r_C	$r_{\Delta A}$	$r_{\Delta B}$	$r_{\Delta C}$	$r_{A\text{-}T}$	$r_{B\text{-}T}$	$r_{C\text{-}T}$		
f_{1AG}	0.973	−0.993	−0.962	0.999	−0.985	−0.990	0.969	−0.998	−0.995	A	12 ms
f_{1BC}	−0.996	0.708	0.909	−0.993	0.956	0.940	−0.998	0.374	0.909	BC	12 ms
f_{1BCG}	−0.987	0.989	0.899	−0.995	0.970	0.988	−0.998	0.280	0.899	BC	12 ms
f_{1ABC}	0.984	0.964	0.960	0.995	0.981	0.990	0.943	0.052	0.960	ABC	12 ms
f_{2AG}	−0.999	−0.988	−0.925	−0.999	−0.940	−0.974	−0.999	−0.997	−0.992	none	/
f_{2BC}	−0.995	−0.939	−0.885	−0.992	−0.884	−0.870	−0.998	−0.999	−0.998	none	/
f_{2BCG}	−0.973	−0.985	−0.977	−0.990	−0.981	−0.940	−0.998	−0.997	−0.998	none	/
f_{2ABC}	−0.999	−0.979	−0.949	−0.998	−0.972	−0.979	−0.999	−0.995	−0.999	none	/
f_{3AG}	−0.997	−0.996	−0.992	−0.998	−0.993	−0.996	−0.999	−0.997	−0.998	none	/
f_{3BC}	−0.997	−0.883	−0.916	−0.995	−0.902	−0.873	−0.999	−0.990	−0.992	none	/
f_{3BCG}	−0.993	−0.974	−0.853	−0.996	−0.975	−0.916	−0.998	−0.982	−0.996	none	/
f_{3ABC}	−0.996	−0.966	−0.907	−0.997	−0.967	−0.955	−0.999	−0.979	−0.997	none	/

interval and the calculated value of $r_{\Phi-T}$ at 20 ms, when the internal fault occurs, reveals that the T/2 time window can effectively improve the protection sensitivity.

B. SIMULATION RESULTS CONSIDERING DIFFERENT TRANSITION RESISTANCES

In order to verify the applicability of the proposed pilot protection principle in the case of high-resistance grounding faults, the simulation verification is conducted on A-phase short-circuits of different transition resistances at f_1 of the tie line. For the doubly-fed power source connected to the power grid, the calculation results of faulty phases r_A and $r_{\Delta A}$ are shown in Fig. 15.

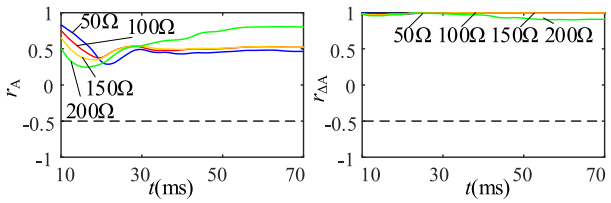

FIGURE 15. Calculation results of r_A and $r_{\Delta A}$ in the case of a a-phase fault at f_1 of tie line.

In Fig. 15, both r_A and $r_{\Delta A}$ under different transition resistances are significantly higher than the protection setpoint after 10 ms (especially $r_{\Delta A}$, which is hardly affected by transition resistance, with the calculated value always close to 1). The protection can operate reliably, demonstrating that the proposed protection scheme has a good ability to respond to high-resistance grounding fault.

C. COMPARISON OF DIFFERENT SIMILARITY ALGORITHMS

Fig. 16 shows the comparison between the similarity criteria proposed in this paper and those in some references (based on Pearson correlation coefficient or cosine similarity, with the time window of 20 ms) in the case of an internal fault. Among them, the fault type is f_{1BC}; the RES provides 20% of the rated

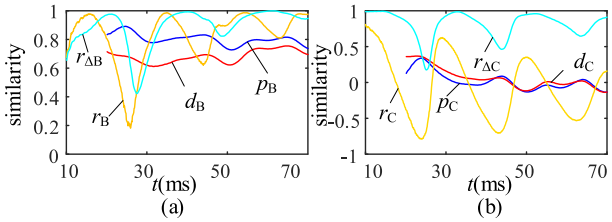

FIGURE 16. Comparison of different similarity criteria in the case of an internal fault.

power before the fault; d_Φ and p_Φ represent the calculation results of the similarity criteria in [17] and [20]; r_Φ and $r_{\Delta\Phi}$ represent the calculation results of criterion proposed in this paper; and the (a) and (b) in Fig. 16 show the comparison results of phase B and phase C, respectively.

According to Fig. 16, relatively speaking, the criteria in this paper improves the protection operation time and sensitivity at the same time: for example, in Fig. 16 (b), the calculated values r_C and $r_{\Delta C}$ of the criteria in this paper are more than 0.8 and 0.9, respectively, at 10 ms; while p_C and d_C are less than 0.4 at 20 ms.

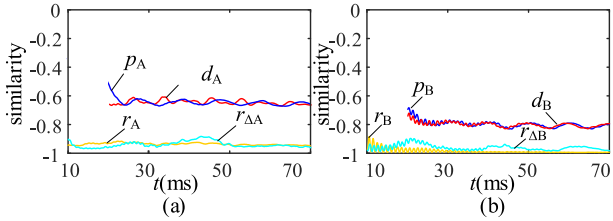

FIGURE 17. Comparison of different similarity criteria in the case of an external fault.

Fig. 17 shows the simulation results of different criteria (taking phase A and B as examples) when the above fault type (BC short circuit) occurs at f_2 outside the tie line. Fig. 17 shows that, due to the capacitive current compensation for the current sampling values in this paper, the calculated values of r_A and $r_{\Delta A}$ of the A-phase criterion are significantly

smaller than those of p_A and d_A, while r_B and $r_{\Delta B}$ of the B-phase criterion are significantly smaller than those of p_B and d_B in the case of external faults. This significantly strengthens the ability of the protection against mis-operation under external faults.

VI. EXPERIMENTAL VERIFICATION

In addition to the simulation verification, the pilot protection is also studied through the experimental platform with a RES.

FIGURE 18. Picture of doubly-fed power source.

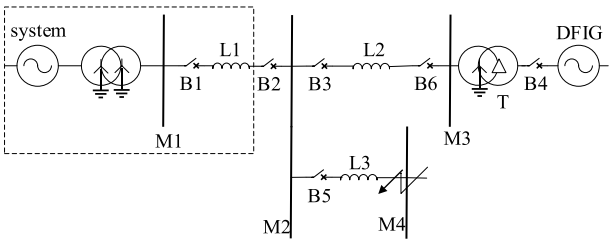

FIGURE 19. Wiring diagram of primary system of experimental platform.

Fig. 18 is the picture of the experimental platform with doubly-fed power source, including the doubly-fed induction generator, back-to-back converter and control cabinet (from left to right). Fig. 19 is the primary wiring diagram of the external system of doubly-fed power source, with the rated voltage of the system power source of 800V, M1-M4 as the busbar (with fault point at M4), B1-B5 as the circuit breaker with measuring unit. The reference direction of current at each measuring point is from the busbar to line. The parameters on the system side measured from B2 are $Z_1 = 6.44\angle 72°\Omega$, $Z_0 = 7.29\angle 60.8°\Omega$. The T transformation ratio is 800V/220V, and the short-circuit impedance is 6%. The rated power of the doubly-fed induction generator is 6kW, the resistance of the rotor and the stator are 170mΩ and 114mΩ respectively, the leakage inductance is 1.44mH, and the mutual inductance is 54mH. The positive-sequence and zero-sequence impedances of line L2 are $Z_1 = 1.2\angle 85°\Omega$ and $Z_0 = 3.0\angle 73°\Omega$, respectively. The positive-sequence and zero-sequence impedances of L3 are $Z_1 = 20.4\angle 82°\Omega$ and $Z_0 = 50.7\angle 74°\Omega$, respectively.

In order to verify the operation of protection scheme in case of internal and external faults at the same time, B3 and B6, and B1 and B6 are formed into 2 groups of pilot protection for verification under different faults on M4. The active power is 0.2 p.u. before the fault. Due to limited space, Table 4 shows the pilot protection comparison results of B1 and B6 in the case of M4 faults (internal faults), while Table 5 shows the pilot protection comparison results of B3 and B6 (external faults).

TABLE 4. Pilot protection comparison results of B1 and B6 in the case of M4 faults.

fault	$r_A / r_{\Delta A}$	$r_B / r_{\Delta B}$	$r_C / r_{\Delta C}$	operation phase
ABC	0.958/0.898	0.941/0.948	0.714/0.990	ABC
BC	-0.965/-0.895	0.925/0.915	0.421/0.978	BC
ABN	0.973/0.997	0.415/0.605	-0.991/-0.992	AB
AN	0.985/0.999	-0.994/-0.992	-0.996/-0.998	A

TABLE 5. Pilot protection comparison results of B3 and B6 in the case of M4 faults.

fault	$r_A / r_{\Delta A}$	$r_B / r_{\Delta B}$	$r_C / r_{\Delta C}$	operation phase
ABC	-0.976/-0.961	-0.978/-0.880	-0.930/-0.901	/
BC	-0.971/-0.861	-0.925/-0.938	-0.912/-0.954	/
ABN	-0.995/-0.998	-0.997/-0.990	-0.998/-0.998	/
AN	-0.998/-0.997	-0.999/-0.999	-0.998/-0.999	/

In Table 4 and Table 5, the calculation results of r_Φ and $r_{\Delta\Phi}$ refer to the maximum values in the 10-20 ms interval after the fault. According to the experimental results, the proposed pilot protection can operate sensitively and reliably under various internal fault conditions. When the external fault occurs, the protection will not operate.

VII. CONCLUSION

This paper proposes a new principle of pilot protection based on the cosine similarity comparison, with the main contributions and conclusions shown as follows:

1) The applicability of traditional current differential protection to the tie line of RES is analyzed. The results show that because the amplitude of short-circuit current provided by RES is limited and the range of phase change is large, when fault occurs in the tie line, the differential current will decrease, the braking current will increase and the protection sensitivity will decrease. In particular, when two-phase short-circuit fault occurs inside the tie line, the phase difference of short-circuit current on both sides of the line may exceed 90° due to the change of short-circuit current distribution characteristics. It may lead to differential protection rejection where the RES capacity has a high proportion, which is difficult to meet the requirements of engineering applications.

2) A new method of pilot protection based on the cosine similarity comparison is proposed. Compared with the traditional current differential protection based on the fundamental frequency component, the pilot protection principle based on the similarity comparison can make full use of the full short-circuit current information such as fundamental and other frequency components, so as to effectively improve the protection sensitivity. Meanwhile,

compared with the existing similarity comparison methods, the proposed method adopts a comprehensive protection scheme combining full short-circuit current and fault component, supplemented by a reasonable selection of time window (T/2 time window), which further improves the protection sensitivity and operation speed.

3) In view of the problems that existing similarity comparison methods usually do not consider the effect of capacitance current, and the traditional phasor-based capacitive current compensation method cannot be applied to the similarity comparison algorithm, a capacitive current compensation method based on Clark transformation is proposed. This method can realize the capacitive current compensation for the short-circuit current sampling value, so as to effectively prevent the protection maloperation in the case of external faults.

4) The simulation and experimental results show that the proposed pilot protection principle is of high sensitivity and fast operation speed, and is suitable for different RESs, which can better meet the engineering application requirements.

The main works in the future are to complete the research of the protection device based on the proposed method of pilot protection and put into the actual power grid after test. In addition, this paper mainly studies the main protection of the tie line of RES: pilot protection. The backup protection of tie line, such as distance protection, also has many problems to be solved, and the related research needs to be in-depth.

REFERENCES

[1] Y. Liang, W. Li, and Z. Lu, "Effect of inverter-interfaced renewable energy power plants on negative-sequence directional relays and a solution," *IEEE Trans. Power Del.*, vol. 36, no. 2, pp. 554–565, Apr. 2021.

[2] D. V. Bozalakov, T. L. Vandoorn, B. Meersman, G. K. Papagiannis, A. I. Chrysochos, and L. Vandevelde, "Damping-based droop control strategy allowing an increased penetration of renewable energy resources in low-voltage grids," *IEEE Trans. Power Del.*, vol. 31, no. 4, pp. 1447–1455, Aug. 2016.

[3] Y. Wen, W. Yang, R. Wang, W. Xu, X. Ye, and T. Li, "Review and prospect of toward 100% renewable energy power systems," *Proc. CSEE*, vol. 40, no. 6, pp. 1843–1856, 2020.

[4] A. Blakers, M. Stocks, B. Lu, C. Cheng, and R. Stocks, "Pathway to 100% renewable electricity," *IEEE J. Photovolt.*, vol. 9, no. 6, pp. 1828–1833, Nov. 2019.

[5] C. Breyer, S. Khalili, D. Bogdanov, M. Ram, A. S. Oyewo, A. Aghahosseini, and A. Gulagi, "On the history and future of 100% renewable energy systems research," *IEEE Access*, vol. 10, pp. 78176–78218, 2022.

[6] S. Yin and J. Wang, "Generation and transmission expansion planning towards a 100% renewable future," *IEEE Trans. Power Syst.*, vol. 37, no. 4, pp. 3274–3285, Jul. 2022.

[7] W. Zappa, M. Junginger, and M. V. D. Broek, "Is a 100% renewable European power system feasible by 2050?" *Appl. Energy*, vols. 233–234, pp. 233–234, Jan. 2019.

[8] G. Song, R. Tao, B. Li, J. Hu, and C. Wang, "Overview of fault analysis and protection of power systems with large-scale electrical & electronic equipment," *Automat. Electr. Power Syst.*, vol. 41, no. 12, pp. 2–12, 2017.

[9] J. Jia, G. Yang, A. H. Nielsen, and P. Rønne-Hansen, "Impact of VSC control strategies and incorporation of synchronous condensers on distance protection under unbalanced faults," *IEEE Trans. Ind. Electron.*, vol. 66, no. 2, pp. 1108–1118, Feb. 2019.

[10] G. Pannell, D. J. Atkinson, and B. Zahawi, "Analytical study of grid-fault response of wind turbine doubly fed induction generator," *IEEE Trans. Energy Convers.*, vol. 25, no. 4, pp. 1081–1091, Dec. 2010.

[11] Y. Li, K. Jia, T. Bi, Y. Sun, and W. Li, "Adaptability analysis of current differential protection in outgoing lines of inverter renewable energy stations," *Automat. Electr. Power Syst.*, vol. 41, no. 12, pp. 100–105, 2017.

[12] C. Wang, G. Song, K. Liu, D. Wang, X. Kang, and Z. Jiao, "Analysis on adaptability of fault component protection to wind power connection systems," *Proc. CSEE*, vol. 34, no. 31, pp. 5485–5492, 2014.

[13] X. Xu and Y. Lu, "A pilot protection scheme suitable for distribution networks with distributed generation," *Automat. Electr. Power Syst.*, vol. 39, no. 9, pp. 113–118, 2015.

[14] J. Li, H. Gao, and G. Zhu, "Inverse-time current differential protection of active distribution network considering characteristics of inverter-based distributed generation," *Trans. China Electrotech. Soc.*, vol. 31, no. 17, pp. 74–83, 2016.

[15] C. Zhou, G. Zou, X. Du, and J. Yang, "Pilot protection of active distribution network based on positive-sequence current fault component," *Proc. CSEE*, vol. 40, no. 7, pp. 2102–2112, 2020.

[16] G. Song, C. Wang, J. Tang, X. Wang, and R. Guo, "A new principle of time domain model identification based pilot protection suitable for wind power connection systems," *Power Grid Technol.*, vol. 40, no. 11, pp. 3580–3585, 2016.

[17] L. Zheng, K. Jia, T. Bi, Y. Fang, and Z. Yang, "Cosine similarity based line protection for large-scale wind farms," *IEEE Trans. Ind. Electron.*, vol. 68, no. 7, pp. 5990–5999, Jul. 2021.

[18] L. Zheng, K. Jia, T. Bi, Z. Yang, and Y. Fang, "A novel structural similarity based pilot protection for renewable power transmission line," *IEEE Trans. Power Del.*, vol. 35, no. 6, pp. 2672–2681, Dec. 2020.

[19] Q. Yang, H. Ma, Y. Liu, and D. Duan, "Novel pilot protection based on time-domain for transmission line with doubly fed induction generator," in *Proc. Int. Trans. Elect. Energy Syst.*, vol. 30, no. 10, 2020, Art. no. e12533.

[20] T. Bi, Y. Li, K. Jia, and Q. Yang, "Pilot protection based on transient current waveform correlation for outgoing lines of renewable energy stations," *Proc. CSEE*, vol. 38, no. 7, pp. 2012–2019, 2018.

[21] K. Jia, Y. Li, Y. Fang, L. Zheng, T. Bi, and Q. Yang, "Transient current similarity based protection for wind farm transmission lines," *Appl. Energy*, vol. 225, pp. 42–51, Sep. 2018.

[22] A.-R. Youssef, E. E. M. Mohamed, and A. I. M. Ali, "Model predictive control for grid-tie wind-energy conversion system based PMSG," in *Proc. Int. Conf. Innov. Trends Comput. Eng. (ITCE)*, Feb. 2018, pp. 467–472.

[23] P. Sochor, N. M. L. Tan, and H. Akagi, "Low-voltage-ride-through control of a modular multilevel single-delta bridge-cell (SDBC) inverter for utility-scale photovoltaic systems," *IEEE Trans. Ind. Appl.*, vol. 54, no. 5, pp. 4739–4751, Sep. 2018.

[24] *Wind Turbines-Test Procedure of Voltage Fault Ride Through Capability*, Standard GB/T 36995-2018, 2018.

[25] R. Kabiri, D. G. Holmes, and B. P. McGrath, "Control of active and reactive power ripple to mitigate unbalanced grid voltages," *IEEE Trans. Ind. Appl.*, vol. 52, no. 2, pp. 1660–1668, Mar./Apr. 2016.

[26] Z. Chang, G. Song, and T. Wang, "Analysis on current characteristics of PMSG under grid three-phase fault," *J. Eng.*, vol. 2018, no. 15, pp. 785–790, Oct. 2018.

[27] X. Kong, Z. Zhang, and X. Yin, "Fault current study of inverter interfaced distributed generators," *Distrib. Gener. Alternative Energy J.*, vol. 30, no. 3, p. 6–26, Jul. 2015.

[28] W.-M. Guo, L.-H. Mu, and X. Zhang, "Fault models of inverter-interfaced distributed generators within a low-voltage microgrid," *IEEE Trans. Power Del.*, vol. 32, no. 1, pp. 453–461, Feb. 2017.

[29] X. Kong, Z. Zhang, X. Yin, F. Wang, and M. He, "Research on fault current characteristics and fault analysis methods of power grid with inverter-based distributed generation," *Proc. CSEE*, vol. 33, no. 34, pp. 65–74, 2013.

[30] X. Guo, W. Wu, and Z. Chen, "Multiple-complex coefficient-filter-based phase-locked loop and synchronization technique for three-phase grid-interfaced converters in distributed utility networks," *IEEE Trans. Ind. Electron.*, vol. 58, no. 4, pp. 1194–1204, Apr. 2011.

[31] Y. He, *Power System Analysis*. Wuhan, China: HUSTP, 2002, pp. 95–130.

[32] Y. Kang, X. Lin, C. Pan, and W. Liu, "Analysis of power transmission characteristics of renewable energy grid-connected converters after SVC and SVG compensation under weak grid conditions," *Proc. CSEE*, vol. 41, no. 6, pp. 2115–2125, 2021.

[33] K. Singh and M. Amir, "Intelligent fuzzy TIDF-II controller for load frequency control in hybrid energy system," *IETE Tech. Rev.*, vol. 2021, pp. 1–17, Nov. 2021.

[34] M. F. Kotb, A. A. El-Fergany, E. A. Gouda, and A. M. Agwa, "Dynamic performance evaluation of photovoltaic three-diode model-based Rung–Kutta optimizer," *IEEE Access*, vol. 10, pp. 38309–38323, 2022.
[35] K. Singh, M. Amir, F. Ahmad, and S. S. Refaat, "Enhancement of frequency control for stand-alone multi-microgrids," *IEEE Access*, vol. 9, pp. 79128–79142, 2021.
[36] Y. Huang, P. Zhou, and L. Wang, "Power control stability of vector control based grid-connected converter under weak grid conditions," *Autom. Electr. Power Syst.*, vol. 40, no. 14, pp. 93–99, 2016.
[37] A. M. A. Haidar, K. M. Muttaqi, and M. T. Hagh, "A coordinated control approach for DC link and rotor crowbars to improve fault ride-through of DFIG-based wind turbine," *IEEE Trans. Ind. Appl.*, vol. 53, no. 4, pp. 4073–4086, Jul. 2017.
[38] J. Ouyang, D. Zheng, X. Xiong, C. Xiao, and R. Yu, "Short-circuit current of doubly fed induction generator under partial and asymmetrical voltage drop," *Renew. Energy*, vol. 88, pp. 1–11, Apr. 2016.
[39] F. Xiao, Z. Zhang, and X. Yin, "Fault current characteristics of the DFIG under asymmetrical fault conditions," *Energies*, vol. 8, pp. 10971–10992, Oct. 2015.
[40] F. Sulla, J. Svensson, and O. Samuelsson, "Symmetrical and unsymmetrical short-circuit current of squirrel-cage and doubly-fed induction generators," *Electr. Power Syst. Res.*, vol. 81, pp. 1610–1618, Jul. 2011.
[41] B. A. Moser, "A similarity measure for image and volumetric data based on Hermann Weyl's discrepancy," *IEEE Trans. Pattern Anal. Mach. Intell.*, vol. 33, no. 11, pp. 2321–2329, Nov. 2011.
[42] J. Suonan, Y. Zhang, J. Qi, and Z. Jiao, "Research on current differential protection based on time domain capacitive current compensation," *J. Xi'an Jiaotong Univ.*, vol. 39, no. 12, pp. 1370–1374, 2005.
[43] P. Jia, Q. Zhang, X. Jia, and C. Wei, "Solution of phase-mode transformation matrix of asymmetric transmission line based on Clarke matrix," *Power Grid Technol.*, vol. 37, no. 9, pp. 2653–2657, 2013.

QINGHUA LAI is currently pursuing the Ph.D. degree with the Huazhong University of Science and Technology (HUST), Wuhan, China. His research interests include operation control and protection technology of large-scale renewable energy power station.

ZHE ZHANG received the Ph.D. degree in electrical engineering from HUST, Wuhan, China, in 1992. Currently, he is a Professor with the College of Electrical and Electronic Engineering, HUST. His research interests include power system analysis and protective relaying.

KANJUN ZHANG received the Ph.D. degree in electrical engineering from HUST, Wuhan, China, in 2008. His research interests include power system analysis and protective relaying.

XIANGGEN YIN (Senior Member, IEEE) received the B.S., M.S., and Ph.D. degrees in electrical engineering from the Huazhong University of Science and Technology (HUST), Wuhan, China, in 1982, 1985, and 1989, respectively. He is currently a Professor with the School of Electrical and Electronic Engineering, HUST. His research interests include power system analysis, fault location, protective relaying, and power system stability control.

YONGXIN CHEN received the M.S.E.E. degree in electrical engineering from HUST, Wuhan, China, in 2020. Her research interests include HVDC systems and power system control and protection.